

Expanding the fracture limits in bulk metal forming to biaxial tension states

Rui Filipe Vieira Sampaio
rui.f.sampaio@tecnico.ulisboa.pt

Instituto Superior Técnico, Universidade de Lisboa, Portugal

November 2021

Abstract: Bulk formability limits in the in-plane principal strain space and in the space of effective strain vs. stress triaxiality are characterized by an uncertainty region in which cracks may be triggered by tension (mode I) or by out-of-plane shear (mode III). The obtainment of experimental data in this region is a long-known problem, hence this document has as main objective the presentation of a new upset bulk formability test geometry that can effectively contribute to the characterization of the formability limits of bulk metal forming in states of biaxial tension, completing the characterization of these limits for the whole range of stress states in which cracking on free surfaces may occur. Moreover, this work also presents an analytical expression for shifting the fracture forming limit line for mode III (OSFFL) in the in-plane principal strain space into a hyperbolic fracture limit curve in the effective strain vs. stress-triaxiality space. The overall utilized methodology combines experimentation together with analytical and numerical modelling. The contents of this work are a step towards reducing the current lack of knowledge regarding failure by fracture in bulk metal forming parts subject to stress triaxiality values beyond uniaxial tension. Results show that a new uncoupled ductile damage criterion built upon the combination of the integrands of the normalized Cockcroft-Latham and McClintock criteria can be successfully used to model the physics of bulk metal forming limits to fracture for the entire range of stress triaxiality values corresponding to fracture initiation on free surfaces.

Keywords: Bulk Formability, Biaxial Tension, Ductile Fracture Mechanics, Damage Mechanics, Experimentation, Finite Element Method.

1. INTRODUCTION

Apart from special purpose metal forming processes in which cracks and formation of new surfaces are needed for the tools to move and for the process to be carried out, such as blanking, piercing, and fine blanking, in all the remaining metal forming processes cracks are undesirable and must be prevented at the design stage. Crack triggering and propagation in metal forming happens as the result of a competition between the accumulation of damage due to tensile stresses, in-plane shear stresses, and out-of-plane shear stresses. These three macroscopic sources of damage are related to the well-known crack opening mechanisms of fracture mechanics: mode I – tension, mode II – in-plane shear, and mode III – out-of-plane shear [1].

For the case of bulk forming, results obtained by Kuhn et al. [2] and plotted in the principal in-plane strain space, $\varepsilon_1 = f(\varepsilon_2)$, showed that the fracture locus in tensile, rolled, and cylindrical upset test specimens fall on a straight line falling from left to right parallel to the loading path of uniaxial compression (refer to the line with slope ‘-1/2’ labelled as ‘1’ in Fig. 1a). Since both vertical and inclined cracks found in the outer surface of the upset compression test specimens do not run radially, one can easily perceive the crack opening mechanism as being based on out-

of-plane shear, as it was originally speculated by Kobayashi [3].

Later, Erman et al. [4] proposed the existence of a bilinear fracture locus resulting from the combination of the fracture limit line of slope ‘-1/2’ and a new fracture limit line of slope ‘-1’ parallel to the loading path of pure shear and labelled as ‘2’ in Fig. 1a. Because this second fracture line is typical of failure by tension (mode I), it may be concluded that loading paths crossing the fracture loci built upon the two straight lines of slope ‘-1/2’ or ‘-1’ will eventually result in failure by fracture with crack opening modes due to out-of-plane shear (mode III) and tension (mode I), respectively.

The link between the above-mentioned failure mechanisms and the critical values of ductile damage was performed by Martins et al. [1], who demonstrated that the slopes ‘-1/2’ and ‘-1’ are directly related to the normalized Cockcroft-Latham [5],[6] and McClintock [7],[8] uncoupled ductile damage criteria, respectively.

Microstructured-based coupled ductile damage criteria (e.g., Tvergaard and Needleman [9]) and macromechanics-based coupled criteria (e.g., Kachanov [10], or Lemaitre [11]) will be left out of this work’s discussion because despite their merits in adjusting the stress response of the materials as a function of the accumulated damage, they do not have an explicit direct link

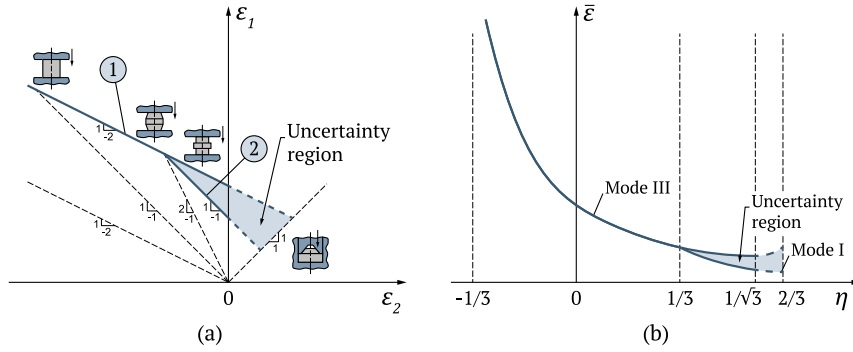


Fig. 1 Schematic representation of the formability limits in (a) the in-plane principal strain space and (b) the space of effective strain vs. stress triaxiality, evidencing the uncertainty region shaded in light blue.

to the three different fracture mechanics' crack opening modes. Additionally, these are more difficult to calibrate due to the relatively large number of parameters involved and have an algebraic treatment that makes them very difficult or even impossible to be handled within the objectives of this paper.

Another type of representation for the bulk metal forming loading paths that has roots in the pioneering works of Hancock and Mackenzie [12] and Vujovic and Shabaik [13] is the effective strain vs. stress-triaxiality space, $\bar{\epsilon} = f(\eta)$, with $\eta = \sigma_m/\bar{\sigma}$. In this alternative representation the fracture loci are given by curved hyperbolic-like lines (Fig. 1b) and are not limited to plane stress loading conditions. The transformation of the fracture locus corresponding to mode I from the principal strain space to the effective strain vs. stress triaxiality space can be performed analytically [14] if plane stress loading conditions are assumed, as it is the case of sheet metal forming. Nevertheless, the plane stress assumption is valid and applicable to cracks being triggered on free surfaces of bulk metal forming parts.

Although recent studies point mostly to the occurrence of failure by tension in bulk metal forming for test samples subjected to states-of-stress in-between uniaxial tension ($\eta = 1/3$) and plane strain ($\eta = 1/\sqrt{3}$) [14], it should not be forgotten that experiments carried out by Kuhn et al. [2] and Gouveia et al. [15] revealed the existence of unique fracture forming limits defined by a single straight line of slope '-1/2', compatible with the normalized Cockcroft-Latham ductile damage criterion and the crack opening mode III (out-of-plane shear). This was perceived by Erman et al. (1983) to vary with both the material and temperature. The two different sets of results give rise to the 'uncertainty region', highlighted in Fig. 1.

Erman et al. [4] addressed this problem in their original paper, concluding that the 'deviations in the small strain region' could be explained by means of the Marciniak and Kuczyński [16] model for localized thinning if two types of small

inhomogeneities were considered in the axial and radial directions. Claiming that the application of this model with inhomogeneities in the radial direction could reproduce the fracture forming line with a slope of '-1/2', they suggested that the inhomogeneities in the axial direction could justify the already mentioned deviations.

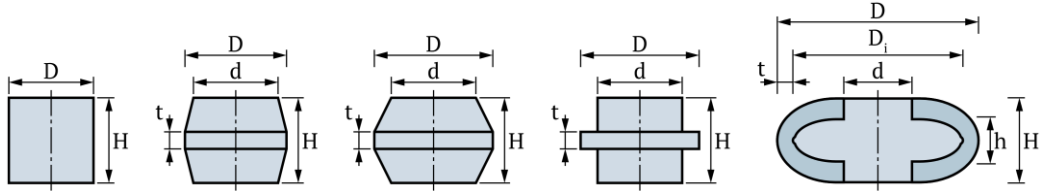
However, this methodology consists of using a localized instability approach directly linked to the plane stress loading conditions of sheet metal forming to the three-dimensional stress loading conditions of bulk metal forming, in which fracture is not preceded by necking. This probably explains the inconclusive circumstances that these authors claimed to determine the application of the model with one type of inhomogeneities over another.

To obtain experimental data in the 'small strain region' of the principal strain space and support the discussion on the deviations of the fracture loci in that region, Erman et al. [4] proposed a partial extrusion test capable of providing equal biaxial tensile strains at fracture. By applying the test to AISI 4640 sintered steel powder at room temperature, they confirmed that the strains at fracture were located on the first quadrant of the principal strain space and close to the fracture forming line with slope '-1/2'. However, the obtained fracture strain values were extremely small and the region where the cracks were triggered is not visible, therefore, making the employment of the state-of-the-art digital image correlation (DIC) systems unsuitable to perform further measurements.

Similar problems of accessibility to DIC systems are found with the ring expansion test specimen developed by Silva et al. [14], which is also capable of providing fracture strains in the first quadrant of the principal strain space. In this case, however, cracks are triggered at the inner ring surface, which is in contact with the die, resulting in negative values of stress triaxiality.

The above discussion justifies the intention of revisiting the fracture forming limits in bulk metal forming under biaxial tension by

Table 1 Geometry and lubrication conditions for the bulk formability test specimens



Geometry (mm)	Cylindrical	Tapered		Flanged	Barreled ring
H	25	25	25	25	50
D	25	30	35	35	170
d	-	25	25	25	90
t	-	5	5	5	6
h	-	-	-	-	28
Di	-	-	-	-	158
Lubrication	Dry	Dry	Dry	Dry	Dry
Identification	c	t1	t2	f	br

presenting an innovative upset test geometry that allows measuring the evolution of strains in a free surface of interest by DIC and by combining the results of these tests with fractography of the cracked surfaces using a scanning electron microscope (SEM). The onset of fracture in the ‘uncertainty region’ is discussed in the light of the fracture forming lines corresponding to crack opening by modes I and III, and a single uncoupled ductile damage criterion is proposed to modulate the material and loading preferences for either of the crack opening modes.

An analytical transformation to convert the fracture forming limit associated to mode III (straight line with slope ‘-1/2’) from the principal strain space into the effective strain vs. stress triaxiality space is also presented for the first time ever. This transformation, together with that earlier developed by Silva et al. [14] to the fracture forming limit associated to mode I will allow for a simple and fast conversion of the fracture loci between the two different spaces.

Finite element simulation using an in-house computer program gives support to the entire presentation.

2. MATERIAL AND METHODS

2.1. Mechanical characterization

The experimental work was performed on commercial aluminum AA7075-T6 that was supplied in the form of solid rods with 200 mm diameter. The flow stress curve in Fig. 2 was determined by means of compression tests carried out on cylindrical test specimens with 25 mm of both height and diameter machined from the rods. The tests were conducted at room temperature on an Instron SATEC 1200 hydraulic testing machine with a constant

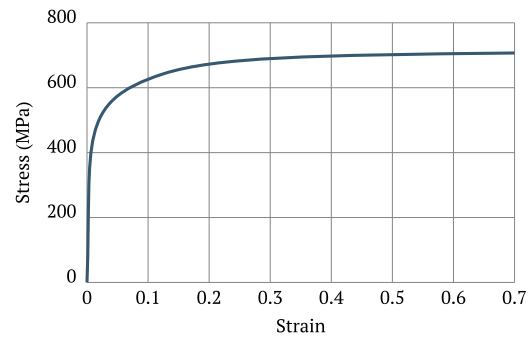


Fig. 2 Flow stress of the AA7075-T6 aluminum alloy.

moving crosshead speed of 5 mm/min (0.083 mm/s).

A molybdenum disulfide (MoS₂) based lubricant was applied on the top and bottom surfaces of the specimens for assurance of near frictionless conditions and the compression platens had an average roughness, R_a , of 0.06 mm.

2.2. Bulk formability tests and methodology

The bulk formability tests were carried out at room temperature on the same hydraulic testing machine that had been used before in the determination of the material flow stress.

Axially-loaded conventional bulk formability specimens (cylindrical, tapered, and flanged) were tested along with the newly proposed test specimen that will be hereafter denoted as the ‘barreled ring specimen’. These were machined from the supplied AA7075-T6 aluminum rods according to the geometries provided in Table 1, and later degreased before being compressed between flat parallel platens with a crosshead speed of 5 mm/min.

As results will show later, the barreled ring specimen allows, for the first time ever in bulk metal forming, for crack triggering under biaxial tension, while allowing for the utilization of DIC

to

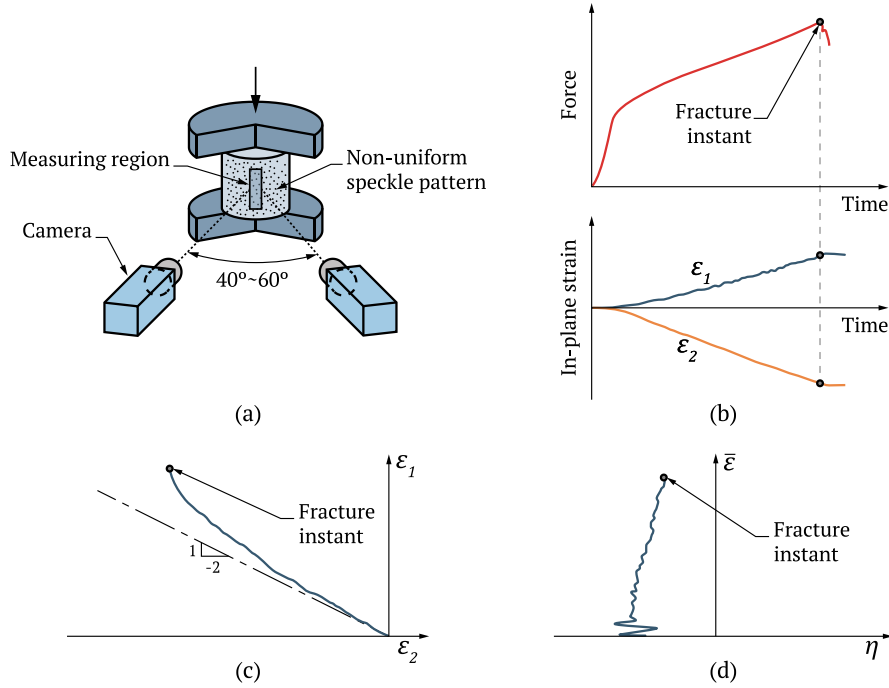


Fig. 3 Methodology to determine and plot the results obtained from the bulk formability tests: (a) schematic representation of the experimental setup utilized in digital image correlation (DIC), (b) combination of the load-time and strain-time evolutions showing the onset of cracking, (c) typical plot of a strain loading path determined by DIC in the principal strain space and (d) alternative representation in the effective strain vs. stress-triaxiality space.

determine the corresponding strains on the outer free surface.

The evolution of the on-surface (in-plane) strains with time during the upset formability tests was determined by means of a *Q-400 3D* DIC system from Dantec Dynamics equipped with two 6-megapixels resolution cameras with 50.2 focal lenses and f/8 aperture (Fig. 3a). For this purpose, the test specimens were made as large as possible to minimize the curvature on the surfaces of interest where the cracks were triggered, and the measurements were performed. These measuring regions were painted in white and subsequently sprayed along the original gauge length with a stochastic black speckle pattern. During testing the measuring regions were illuminated with a spotlight and images were acquired with a frequency of 10 Hz (10 images per second).

Combining the evolutions of the on-surface strains and the upset force with time, the exact instant of time at which cracks were triggered was acquired (see Fig. 3b). This experimental procedure was developed by Magrinho et al. [17] and relies on the fact that a drop in the upset force marks the onset of cracking. The following crack propagation comes also with a sudden relief of stresses which makes it impossible for the DIC system to correlate the digital images obtained from the cracked regions of the specimens with accuracy.

The evolution of the strain loading paths in the principal strain space, $\epsilon_1 = f(\epsilon_2)$, (Fig. 3c) is then computed by combining the evolutions of the

major and minor strains with time. The alternative evolutions in the strain vs. stress-triaxiality space, $\bar{\epsilon} = f(\eta)$, (Fig. 3d) are obtained from the transformation of the loading paths assuming plane stress conditions, which is valid for the free outer surfaces where cracks are triggered.

2.3. Numerical simulation

Numerical simulations of the newly proposed specimen geometry were performed with the finite element computer program *i-form*, an in-house software built upon the irreducible finite element flow formulation [18]. The specimens were assumed as deformable, isotropic, rotationally symmetric objects and their cross sections were discretized by means of quadrilateral elements. Refinement of the meshes in the regions where cracks are triggered and subsequently propagated were performed by means of a quadtree subdivision strategy.

Fig. 4 includes an example of the finite element model utilized in the numerical simulation of the barreled ring at the beginning and end of testing. The model contains approximately 5600 elements, and the simulation took approximately 1h to be finished on a standard laptop equipped with an Intel i5-7200U CPU (2.5 GHz) processor.

The compression platens were modelled as rigid objects and their contour was discretized by means of linear contact-friction elements. Friction was included by means of the law of

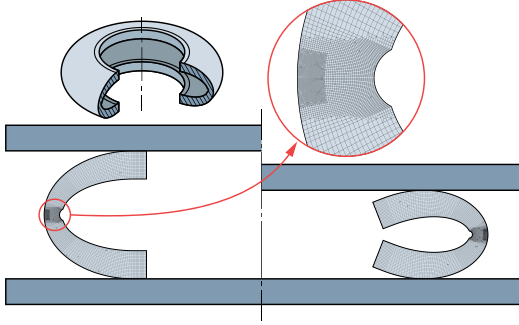


Fig. 4 Finite element model of the upsetting of the new barreled ring specimen at the beginning (left) and end of testing (right) with a detail of the region of interest where cracks are triggered and propagated.

constant friction, $\tau_f = mk$, where k is the shear flow stress and m is the friction factor. A value of m equal to 0.1 was used after checking the finite element predicted forces that best matched the experimental measurements.

The accumulation of ductile damage for the test specimens that exhibit cracking by tension (mode I), D^{Mc} , was calculated by means of the uncoupled criterion due to McClintock [7],[8], whereas the accumulation of ductile damage for the test specimens that exhibit cracking by out-of-plane shear (mode III), D^{NCL} , was determined by means of the normalized Cockcroft-Latham [5],[6] uncoupled damage criterion. Both criteria are included in the finite element computer program by means of the following expressions,

$$D^{Mc} = \int_0^{\bar{\epsilon}} \frac{\sigma_m}{\bar{\sigma}} d\bar{\epsilon} \quad (1)$$

$$D^{NCL} = \int_0^{\bar{\epsilon}} \frac{\sigma_1}{\bar{\sigma}} d\bar{\epsilon} \quad (2)$$

where σ_m is the hydrostatic stress, $\bar{\sigma}$ is the effective stress, σ_1 is the major principal stress, and $\bar{\epsilon}$ is the effective strain.

3. RESULTS AND DISCUSSION

3.1. Formability limits in the principal strain space

The experimental strain loading paths up to fracture were determined according to the methodology described in Section 2.2, which combines the in-plane principal strains vs. time evolutions obtained from DIC with the force vs. time evolutions obtained from the load cell. Fig. 5a, includes these results for the new barreled ring test specimen.

The experimental strain loading paths up to fracture that were determined from DIC for the entire set of formability tests that are listed in Table 1 are shown in Fig. 5b. As seen, the fracture strains on the free surfaces of the cylindrical and of the four different tapered test specimens fall on a line with a slope equal to '-1/2' and

related to crack opening by out-of-plane shear (mode III), which is in close agreement with the one obtained by Oh and Kobayashi [19] for AA7075-T6 aluminum alloy, whereas the two flanged test specimens fall on a line with a slope equal to '-1' and related to crack opening by tension (mode I). These results point out to the existence of a bilinear fracture locus, as it was originally proposed by Erman et al. [4] and recently confirmed by Silva et al. [14].

The problem with the bilinear fracture loci concept is the results obtained for the new barreled ring test specimen, which do not fall on any of the above-mentioned fracture forming limit lines. In fact, the strain values of fracture obtained for this specimen are located above the fracture forming line with slope '-1/2'.

This non-compliance of the barreled ring with either crack opening mode fracture forming limit line manifests the existence of an 'uncertainty region' that can slightly spread beyond the triangular area limited by the two fracture forming lines (see Fig. 1) corresponding to the McClintock (mode I) and normalized Cockcroft-Latham (mode III) damage criteria, suggesting a competition between fracture modes. There is, therefore, a need to investigate the possibility of developing a single uncoupled ductile damage criterion for bulk metal forming that can replicate the loading condition preferences for either of the crack opening modes or for the combination of the crack opening modes within the uncertainty region.

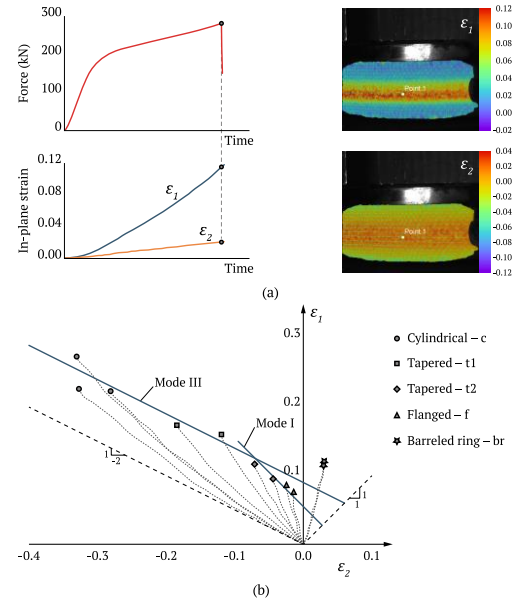


Fig. 5 (a) Summary of the methodology for determining the strain loading paths up to fracture for the new barreled ring specimen and (b) the strain loading paths and strain values at fracture for the entire set of tests listed in Table 1. Note: the images of DIC correspond to the instant of time immediately before fracture and 'Point 1' is the location where cracks were triggered.

3.2. Formability limits in the effective strain vs. stress triaxiality space

The loading paths can alternatively be plotted in the effective strain vs. stress-triaxiality space, $\bar{\epsilon} = f(\eta)$. By focusing only on the fracture strains, the transformation of the straight fracture forming limit line with slope '-1' (mode I) from the principal strain space to the effective strain vs. stress-triaxiality space can be performed analytically by means of the following expression derived in [14],

$$\bar{\epsilon}_f = \frac{2(\epsilon_{\theta f} + \epsilon_{zf})}{3} \frac{D_{crit}^{Mc}}{\eta} = \frac{D_{crit}^{Mc}}{\eta} \quad (3)$$

The above expression gives rise to a hyperbolic fracture forming limit, where the subscript 'f' is utilized for the different strains at fracture and the subscript 'crit' is used for the critical accumulated value of damage up to fracture.

Following a similar approach, the transformation of the straight fracture forming limit line with slope '-1/2' (mode III) can be expressed as follows (refer to equation (2), under the assumption of proportional strain loading paths),

$$\bar{\epsilon}_f = \frac{D_{crit}^{NCL}}{\sigma_1/\bar{\sigma}} \quad (4)$$

where D_{crit}^{NCL} is the critical value of accumulated damage according to the normalized Cockcroft-Latham ductile damage criterion.

However, equation (4) is not adequate to perform the required transformation from the principal strain space into the effective strain vs. stress-triaxiality space because it does not include an explicit dependency on stress-triaxiality $\eta = \sigma_m/\bar{\sigma}$.

To obtain such an expression, one must start from the following equation for the $\sigma_1/\bar{\sigma}$ ratio given in [1] and applicable for isotropic metallic materials under the Levy-Mises constitutive equations,

$$\frac{\sigma_1}{\bar{\sigma}} = \frac{\eta}{\sigma_m/\sigma_1} = \frac{2 + \beta}{(1 + \beta)} \eta \quad (5)$$

Then, it is necessary to write the strain loading path slope $\beta = d\epsilon_2/d\epsilon_1$ as a function of the stress-triaxiality η . This full derivation is included in Appendix A and eventually allows writing the $\sigma_1/\bar{\sigma}$ ratio as a function of η (Fig. 6),

$$\frac{\sigma_1}{\bar{\sigma}} = \frac{(27\eta^2 - 6) - 3\eta\sqrt{-3(9\eta^2 - 4)}}{9\eta^2 - 3\eta\sqrt{-3(9\eta^2 - 4)}} \eta \quad (6)$$

By replacing (6) into (5), the required transformation of the straight fracture forming limit line with slope '-1/2' from the principal strain space into the effective strain vs. stress-triaxiality space is obtained as,

$$\bar{\epsilon}_f = \left(\frac{9\eta^2 - 3\eta\sqrt{-3(9\eta^2 - 4)}}{(27\eta^2 - 6) - 3\eta\sqrt{-3(9\eta^2 - 4)}} \right) \frac{D_{crit}^{NCL}}{\eta} \quad (7)$$

The resulting fracture forming limit corresponding to mode III is also hyperbolic-like, but the

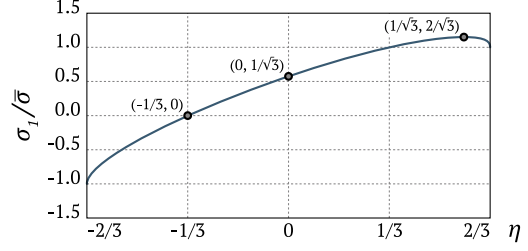


Fig. 6 Variation of the $\sigma_1/\bar{\sigma}$ ratio with stress triaxiality.

asymptote is in $\eta = -1/3$ and not in $\eta = 0$, as it is for the case of mode I (3).

Fig. 7 includes the fracture forming limits corresponding to cracking by modes I and III after being transformed from the principal strain space to the effective strain vs. stress-triaxiality space together with the values of the effective strain at fracture obtained for the entire set of tests listed in Table 1.

As seen, the bilinear fracture loci concept is suitable to model all the different test specimens apart from the new barreled ring. This requires a closer look at the deformation mechanics of this specimen in the following section.

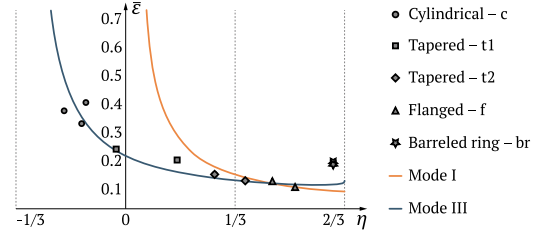


Fig. 7 Representation of the fracture loci corresponding to cracking by mode I and III together with the values of effective strain at fracture for the entire set of test cases included in Table 1.

3.3. Deformation mechanics of the new barreled ring specimen

The fracture initiation site of the new barreled ring specimen is located on the equatorial free surface and is not covered by dies or other tool parts. This allows employing the DIC system to measure the strain loading paths up to failure by fracture during the entire formability tests.

Fig. 8a and 8b show the finite element predicted distributions of the longitudinal, σ_z , and radial, σ_r , stresses at the onset of fracture. As seen, $\sigma_z > 0$ on the outer equatorial free surface due to a bending moment created by the compressive forces acting on the upper and bottom surfaces of the ring (refer to the black arrows in Fig. 8a). This result combined with the circumferential tensile stresses, $\sigma_\theta > 0$, originated by ring expansion during upsetting proves that the barreled ring specimen is in fact subjected to biaxial tension on the outer equatorial free surface where the cracks are triggered.

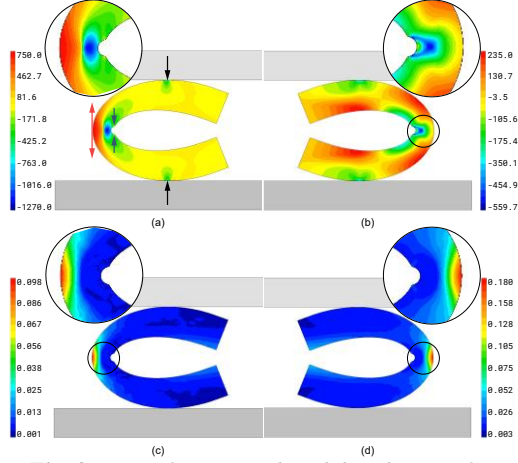


Fig. 8 Finite element predicted distribution of (a) longitudinal stress, σ_z , (b) radial stress, σ_r , (c) ductile damage according to the McClintock criterion and (d) ductile damage according to the normalized Cockcroft-Latham criterion.

Conversely, the distribution of σ_r (Fig. 8b) confirms the existence of plane stress loading conditions, $\sigma_r = 0$, on the outer and inner equatorial free surfaces, and the presence of values $\sigma_r \neq 0$ within the wall thickness. This last result ($\sigma_r \neq 0$) is important because it indicates that the barreled ring specimen can replicate the three-dimensional stress states that are typical of bulk metal forming.

Since, according with the proposed definition of uncertainty region, fracture in this region may be triggered by either tension (mode I) or through-thickness shear (mode III), Fig. 8c and Fig. 8d show the finite element predicted distribution of damage according to the McClintock and normalized Cockcroft-Latham criteria, respectively. Results show that both criteria can correctly predict the region of the specimen where the cracks are triggered, but their maximum accumulated values of damage are greater than the critical damages at fracture derived from the biaxial fracture loci of Fig. 7. For instance, for the case of the normalized Cockcroft-Latham criterion, $D_{max}^{NCL} = 0.18$ while the fracture locus of mode III corresponds to $D_{crit}^{NCL} = 0.10$. For the McClintock criteria the values are $D_{max}^{Mc} = 0.10$ and $D_{crit}^{Mc} = 0.04$.

Despite the above-mentioned differences between the maximum accumulated and the critical values of damage at fracture for the normalized Cockcroft-Latham criterion, the crack opening mode by out-of-plane shear (mode III) is compatible with the numerical and scanning electron microscope (SEM) observations. This is shown in Fig. 9b where finite elements predict an inclined onset of fracture typical of crack opening by out-of-plane shear (mode III) and the picture from SEM (refer to ‘A’ in Fig. 9c) shows a smooth cracked surface typical of shear.

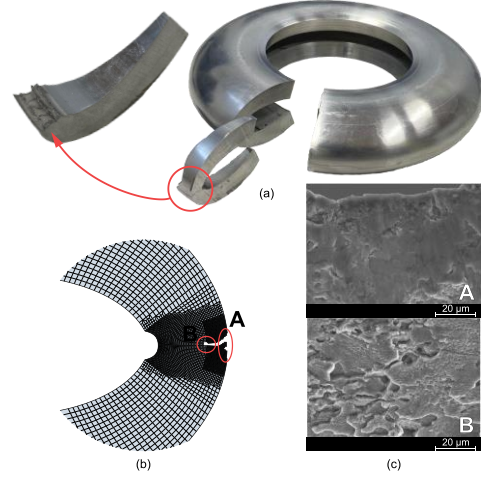


Fig. 9 (a) Picture of the barreled ring specimen after cracking, (b) finite element predicted onset and propagation of cracks and (c) fractography details disclosing crack opening by out-of-plane shear and subsequent propagation by tension.

Further crack propagation along the radial direction and the corresponding images from SEM (refer to ‘B’ in Fig. 9c) showing signs of a dimple-based morphology are compatible with a tension-based mechanism (mode I).

3.4. A new uncoupled ductile damage criterion for bulk forming

The main conclusion derived from Fig. 7 is that neither the McClintock (mode I) nor the normalized Cockcroft-Latham (mode III) ductile damage criteria can replicate the experimental values of effective strain at fracture $\bar{\epsilon}_f$ for the entire range of stress-triaxiality values $-1/3 \leq \eta \leq 2/3$.

As seen, the normalized Cockcroft-Latham criterion works well in the range $-1/3 \leq \eta < 1/3$, where cracks are triggered by out-of-plane shear (mode III), and the McClintock criterion works well in the range $1/3 \leq \eta \leq 1/\sqrt{3}$, where cracks are triggered by tension (mode I). However, none of the criteria is successful in replicating the effective strain at fracture $\bar{\epsilon}_f$ of the new barreled ring specimen (where, $1/\sqrt{3} < \eta \leq 2/3$), because the experimental values surpass the fracture locus corresponding to modes I and III.

In addition to what was said above, the suitability of the McClintock criterion for the range $1/3 \leq \eta \leq 1/\sqrt{3}$ can be called into question due to the work of Kuhn et al. [2], which points out to a single rather than dual fracture locus.

The previously mentioned ‘uncertainty region’ is the result of all these contradictory results that have been reported in the literature since the early 1970’s plus the difficulty in modelling the experimental values of $\bar{\epsilon}_f$ obtained with the new barreled ring specimen. Thus, a new uncoupled

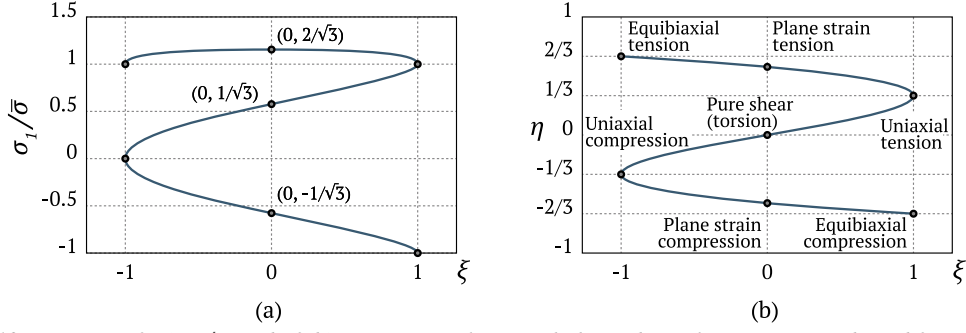


Fig. 10 Variation of (a) $\sigma_1/\bar{\sigma}$ and of (b) stress-triaxiality η with the Lode angle parameter (adapted from [22]).

ductile damage criterion is needed to properly handle the fracture forming limits of bulk forming for $\eta \geq 1/3$.

A recent work [20] focused on the development of a ductile damage criterion that works for the entire range of stress-triaxiality values suggests the combination of the integrands $\tau_{max}/\bar{\sigma}$ and $\sigma_1/\bar{\sigma}$ of the normalized maximum shear and normalized Cockcroft-Latham criteria, as follows,

$$\left(C_1 \left(\frac{\tau_{max}}{\bar{\sigma}} \right) + (1 - C_1) \left(\frac{\langle \sigma_1 \rangle}{\bar{\sigma}} \right) \right)^{c_2} \bar{\epsilon}_f = \left(C_1 \left(\frac{1}{\sqrt{3}} \cos \left[\frac{\pi}{6} \bar{\theta} \right] \right) + (1 - C_1) \left(\frac{\langle 3\eta + 2\cos \left[\frac{\pi}{6} (1 - \bar{\theta}) \right] \rangle}{3} \right) \right)^{c_2} \bar{\epsilon}_f = C_3 \quad (8)$$

where C_i are parameters to be experimentally determined and $\bar{\theta}$ is the normalized Lode angle.

Another recently proposed uncoupled damage criterion [21] results of the combination of the normalized Cockcroft-Latham and maximum shear criteria, with the authors claiming these are responsible for the coalescence of voids under tension and shear, respectively, and adding an exponential function of stress triaxiality to model void growth as follows, where C_i are parameters to be experimentally determined,

$$\left[\left(\frac{2\tau_{max}}{\bar{\sigma}} \right)^{c_1} + \left(\frac{\sigma_1}{\bar{\sigma}} - 1 \right) \right]^{c_2} \exp \left(C_3 \left(\eta - \frac{1}{3} \right) \right) \bar{\epsilon}_f = C_4 \quad (9)$$

However, due to the relation between the normalized Cockcroft-Latham criterion and the crack opening mechanism by out-of-plane shear, it may be concluded that the physics behind (8) is based on a weighted combination of two shear-based criteria. The same happens for (9), along with the fact that the stated control mechanisms of void growth and coalescence are not compatible with the theory developed by McClintock [8], where voids grow and coalesce controlled by the same parameters in the two stages, whether this happens because of tension, shear, or a combination of both.

Still, equation (8) is interesting because it provides a direct link between the integrand $\sigma_1/\bar{\sigma}$ of the normalized Cockcroft-Latham criterion and the normalized Lode angle $\bar{\theta}$, which can be rewritten in terms of the Lode angle parameter ξ , as follows,

$$\frac{\sigma_1}{\bar{\sigma}} = \frac{3\eta + 2\cos \left[\frac{\pi}{6} (1 - \bar{\theta}) \right]}{3} = \eta + \frac{2}{3} \cos \left(\frac{\cos^{-1} \xi}{3} \right) \quad (10)$$

The graphical representation of (10) is shown in Fig. 10 and has some similarities with the relation between the stress-triaxiality, η , and the Lode angle parameter [22], ξ , which is included in the figure for comparison purposes. However, in contrast to $\eta = f(\xi)$, it may be concluded that $\sigma_1/\bar{\sigma} = f(\xi)$ is not a true function for stress states beyond uniaxial tension (i.e., for $\sigma_1/\bar{\sigma} > 1$ or, $1/3 \leq \eta \leq 2/3$) because different values of ξ can result in the same values of $\sigma_1/\bar{\sigma}$.

Since the concept of fracture mode competition suggests an intertwining of mode I and III beyond uniaxial tension, similar to what was proposed in [20] and [21], a new uncoupled ductile damage criterion may be proposed by combining the integrands of different criteria, one of them being the normalized Cockcroft-Latham one, since it presents a great suitability for out-of-plane shear-triggered cracking ($-1/3 \leq \eta < 1/3$). However, instead of using two shear-based criteria, a function that accounts for the dilatational effects on void growth and coalescence (that are directly related with crack opening by tension) should be considered when these effects start to be relevant ($\eta \geq 1/3$ – the uncertainty region). This justifies the following expression for the critical value of accumulated damage D_{crit}^{new} of the new criterion,

$$D_{crit}^{new} = \int_0^{\bar{\epsilon}_f} \frac{\sigma_1}{\bar{\sigma}} d\bar{\epsilon} + C \int_0^{\bar{\epsilon}_f} \left(\eta - \frac{1}{3} \right)^2 d\bar{\epsilon} \quad (11)$$

where C is a parameter to be determined from experiments, and the second term in the right-hand side is a modified version of the McClintock criterion which is only active in the ‘uncertainty region’ and that can ensure a smooth transition with the remaining fracture locus modelled by the normalized Cockcroft-Latham

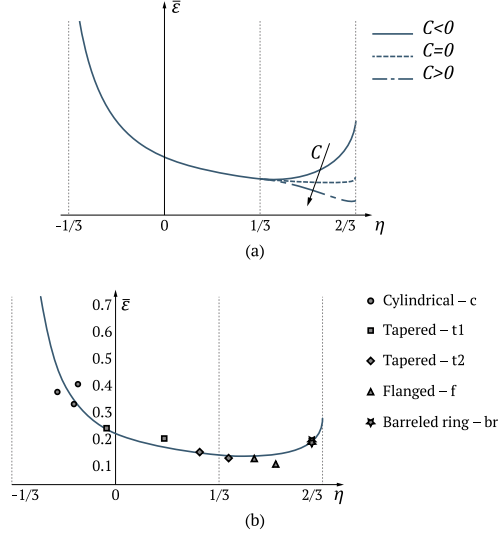


Fig. 11 (a) Schematic representation of the new proposed ductile damage criterion in the effective strain vs. stress-triaxiality space and (b) application of the new criterion to the test specimens of Table 1.

criterion. The influence of C in the overall shape of the fracture locus is schematically disclosed in Fig. 11a.

Regarding the modified version of the McClintock criterion by means of a quadratic term, it is worth noticing that Tai and Yang [23] also made use of such a term in the development of a damage criterion in which the weighting function is based on Lemaitre's [11] definition of strain energy release rate associated to fracture initiation by means of void growth and coalescence.

Fig. 11b presents the application of the new proposed criterion with a value of $C = -4.96$ to the entire set of experimental test cases of Table 1. The critical damage $D_{crit}^{new} = 0.11$ resulting from (11) allows establishing a fracture locus that is in good agreement with the experimental data and that proves the feasibility of using a single criterion to define the formability limits by fracture in bulk metal forming.

4. CONCLUSIONS

Upset formability tests performed with a new 'barreled ring' geometry in conjunction with digital image correlation (DIC) measurements allow determining the experimental strains at fracture in bulk metal forming under biaxial tension. Combination of these results with others available in the literature clearly show that failure by cracking on the free surfaces of bulk metal forming parts subjected to stress-triaxiality values beyond uniaxial tension is characterized by a competition between the opening mode I (by tension) and the opening mode III (by out-of-plane shear). The new barreled ring specimen is

a good example of this competition because cracks are triggered by shear and propagate radially by tension.

The new uncoupled ductile damage criterion built upon the integrand of the normalized Cockcroft-Latham criterion corresponding to crack opening by mode III and the modified integrand of the McClintock criterion related to crack opening by mode I, can surpass the difficulties of each individual criteria in modelling the formability limits of bulk metal forming for the entire range of stress-triaxiality values. The parameter C included in the new uncoupled ductile damage criterion is responsible for adapting its critical value at fracture as a function of the single or dual crack opening modes that characterize the 'uncertainty region' with stress-triaxiality values beyond uniaxial tension.

A new analytical expression for converting the fracture forming limits by mode III from principal strain space into the effective strain vs. stress-triaxiality space is also derived so that, together with a previously derived expression for mode I, can be used for the entire range of stress-triaxiality values.

APPENDIX A

Stress-triaxiality, η , can be written in terms of the strain loading path slope, β , for plane stress loading conditions prevailing on the free bulk forming surfaces where cracks are triggered,

$$\eta = \frac{(1 + \beta)}{\sqrt{3}\sqrt{1 + \beta + \beta^2}} \Rightarrow \frac{1 + \beta + \beta^2}{(1 + \beta)^2} = \frac{1}{3\eta^2} \quad (\text{A1})$$

Simplifying the left-term on the right-hand side,

$$\beta + \frac{1}{\beta} = -2 \frac{9\eta^2/2 - 3}{9\eta^2 - 3} = f(\eta) \quad (\text{A2})$$

Multiplying the left- and right-hand sides of (A2) by β , results in the following quadratic equation,

$$\beta^2 - f(\eta) \times \beta + 1 = 0 \quad (\text{A3})$$

Because the strain loading paths vary between uniaxial compression and equal biaxial tension, $-2 \leq \beta \leq 1$ when $-1/3 \leq \eta \leq 2/3$. This relation between the strain loading path slope β and the stress-triaxiality η allows concluding that only the following solution of (A3) is physically admissible,

$$\beta = \frac{-2(9\eta^2/2 - 3) - 6\eta\sqrt{-(9\eta^2/4 - 1)3}}{2(9\eta^2 - 3)} \quad (\text{A4})$$

(A4) can now be introduced into equation (5) of Section 3.2 to obtain equation (6). The latter can then be introduced into equation (4) of Section 3.2, resulting in equation (7), allowing for the expression of the effective strain at fracture $\bar{\epsilon}_f$ as

a function of the stress-triaxiality η for mode III (out-of-plane shear) of fracture mechanics.

REFERENCES

- [1] Martins, P. A. F., Bay, N., Tekkaya, A. E., & Atkins, A. G. (2014). Characterization of fracture loci in metal forming. *International Journal of Mechanical Sciences*, 83, 112–123. <https://doi.org/10.1016/j.ijmecsci.2014.04.003>.
- [2] Kuhn, H. A., Lee, P. W., & Erturk, T. (1973). A Fracture Criterion for Cold Forming. *Journal of Engineering Materials and Technology*, 95(4), 213–218. <https://doi.org/10.1115/1.3443155>.
- [3] Kobayashi, S. (1970). Deformation Characteristics and Ductile Fracture of 1040 Steel in Simple Upsetting of Solid Cylinders and Rings. *Journal of Engineering for Industry*, 92(2), 391–398. <https://doi.org/10.1115/1.3427752>.
- [4] Erman, E., Kuhn, H. A., & Fitzsimons, G. (1983). Novel Test Specimens for Workability Testing. In R. Chait & R. Papirno (Eds.), *Compression Testing of Homogeneous Materials and Composites* (pp. 279–290). West Conshohocken, PA: ASTM International. <https://doi.org/10.1520/STP36209S>.
- [5] Oh, S. I., Chen, C. C., & Kobayashi, S. (1979). Ductile Fracture in Axisymmetric Extrusion and Drawing—Part 2: Workability in Extrusion and Drawing. *Journal of Engineering for Industry*, 101(1), 36–44. <https://doi.org/10.1115/1.3439471>.
- [6] Cockcroft, M. G., & Latham, D. J. (1968). Ductility and the Workability of Metals. *Journal of the Institute of Metals*, 96, 33–39.
- [7] Ayada, M., Higashino, T., & Mori, K. (1987). Central Bursting in Extrusion of Inhomogeneous Materials. *Proceedings of the Second International Conference on Technology of Plasticity, Vol. 1*, 553–558. Stuttgart.
- [8] McClintock, F. A. (1968). A Criterion for Ductile Fracture by the Growth of Holes. *Journal of Applied Mechanics*, 35(2), 363–371. <https://doi.org/10.1115/1.3601204>.
- [9] Tvergaard, V., & Needleman, A. (1984). Analysis of the cup-cone fracture in a round tensile bar. *Acta Metallurgica*, 32(1), 157–169. [https://doi.org/10.1016/0001-6160\(84\)90213-X](https://doi.org/10.1016/0001-6160(84)90213-X).
- [10] Kachanov, L. M. (1958). О времени разрушения в условиях ползучести [Rupture time under creep conditions]. *Izvestiya Akademii Nauk SSSR, Otdelenie Tekhnicheskikh Nauk*, 8, 26–31. <https://doi.org/10.1023/A:1018671022008>.
- [11] Lemaitre, J. (1985). A Continuous Damage Mechanics Model for Ductile Fracture. *Journal of Engineering Materials and Technology*, 107(1), 83–89. <https://doi.org/10.1115/1.3225775>.
- [12] Hancock, J. W., & Mackenzie, A. C. (1976). On the mechanisms of ductile failure in high-strength steels subjected to multi-axial stress-states. *Journal of the Mechanics and Physics of Solids*, 24, 147–169. [https://doi.org/10.1016/0022-5096\(76\)90024-7](https://doi.org/10.1016/0022-5096(76)90024-7).
- [13] Vujovic, V., & Shabaik, A. H. (1986). A New Workability Criterion for Ductile Metals. *Journal of Engineering Materials and Technology*, 108(3), 245–249. <https://doi.org/10.1115/1.3225876>.
- [14] Silva, C. M. A., Alves, L. M., Nielsen, C. V., Atkins, A. G., & Martins, P. A. F. (2015). Failure by fracture in bulk metal forming. *Journal of Materials Processing Technology*, 215, 287–298. <https://doi.org/10.1016/j.jmatprotec.2014.08.023>.
- [15] Gouveia, B. P. P. A., Rodrigues, J. M. C., & Martins, P. A. F. (1996). Fracture predicting in bulk metal forming. *International Journal of Mechanical Sciences*, 38(4), 361–372. [https://doi.org/10.1016/0020-7403\(95\)00069-0](https://doi.org/10.1016/0020-7403(95)00069-0).
- [16] Marciniak, Z., & Kuczyński, K. (1967). Limit strains in the processes of stretch-forming sheet metal. *International Journal of Mechanical Sciences*, 9(9), 609–620. [https://doi.org/10.1016/0020-7403\(67\)90066-5](https://doi.org/10.1016/0020-7403(67)90066-5).
- [17] Magrinho, J. P., Silva, M. B., Alves, L. M., Atkins, A. G., & Martins, P. A. F. (2018). New methodology for the characterization of failure by fracture in bulk forming. *The Journal of Strain Analysis for Engineering Design*, 53(4), 242–247. <https://doi.org/10.1177/0309324718758842>.
- [18] Nielsen, C. V., & Martins, P. A. F. (2021). *Metal Forming: Formability, Simulation, and Tool Design* (1st ed.). New York, NY: Academic Press.
- [19] Oh, S. I., & Kobayashi, S. (1976). Workability of aluminum alloy 7075-T6 in upsetting and rolling. *Journal of Manufacturing Science and Engineering*, 98(3), 800–806. <https://doi.org/10.1115/1.3439032>.
- [20] Cerik, B. C., & Choung, J. (2020). Ductile Fracture Behavior of Mild and High-Tensile Strength Shipbuilding Steels. *Applied Sciences*, 10(20). <https://doi.org/10.3390/app10207034>.
- [21] Li, X., Yang, W., Xu, D., Ju, K., & Chen, J. (2021). A new ductile fracture criterion considering both shear and tension mechanisms on void coalescence. *International Journal of Damage Mechanics*, 30(3), 374–398. <https://doi.org/10.1177/1056789520962831>.
- [22] Bai, Y., & Wierzbicki, T. (2008). A new model of metal plasticity and fracture with pressure and Lode dependence. *International Journal of Plasticity*, 24(6), 1071–1096. <https://doi.org/10.1016/j.ijplas.2007.09.004>.
- [23] Tai, W. H., & Yang, B. X. (1987). A new damage mechanics criterion for ductile fracture. *Engineering Fracture Mechanics*, 27(4), 371–378. [https://doi.org/10.1016/0013-7944\(87\)90174-3](https://doi.org/10.1016/0013-7944(87)90174-3).